
**Separation Science and Technology**
Publication details, including instructions for authors and subscription information:
http://www.informaworld.com/smpp/title~content=t713708471

# A Methodology for the Characterization of Ion-Exchange Resins

Venkatesh Natarajan[a]; Steven Cramer[a]
[a] DEPARTMENT OF CHEMICAL ENGINEERING, RENSSELAER POLYTECHNIC INSTITUTE, TROY, NEW YORK, USA

Online publication date: 28 August 2000

**To cite this Article** Natarajan, Venkatesh and Cramer, Steven(2000) 'A Methodology for the Characterization of Ion-Exchange Resins', Separation Science and Technology, 35: 11, 1719 — 1742
**To link to this Article: DOI:** 10.1081/SS-100102490
**URL:** http://dx.doi.org/10.1081/SS-100102490

SEPARATION SCIENCE AND TECHNOLOGY, **35**(11), pp. 1719–1742, 2000

# A Methodology for the Characterization of Ion-Exchange Resins

VENKATESH NATARAJAN and STEVEN CRAMER*
DEPARTMENT OF CHEMICAL ENGINEERING
RENSSELAER POLYTECHNIC INSTITUTE
TROY, NEW YORK 12180-3590, USA



## ABSTRACT

Tremendous strides have been made in the field of stationary phase synthesis over the course of the last decade. Although important research has been carried out to elucidate the characteristics of various resins, there is currently a lack of understanding regarding the effect of the various resin materials on preparative modes of chromatography. To describe preparative chromatography, one needs to have appropriate isotherm and transport models. In this article a methodology is presented to enable the identification of appropriate transport models to describe the chromatographic behavior of solutes in preparative ion-exchange systems. The methodology involves simple pulse experiments to estimate the various transport parameters followed by the construction and analysis of various dimensionless groups to identify the dominant transport mechanisms in a given resin. Following this, one can identify an appropriate transport model to describe the chromatographic behavior of solutes on the resin material. This model is then employed in concert with the steric mass action (SMA) isotherm and is validated using experimental data. The results presented provide significant insight into the identification of dominant transport mechanisms on various ion-exchange resin systems.

## INTRODUCTION

Chromatography is widely employed in the biotechnology industry as a preparative tool. The performance of chromatographic systems is highly dependent on the characteristics of the resin being employed for the separation.

* To whom correspondence should be addressed.

The characteristics that one desires in a resin for a preparative application are capacity, selectivity, and rapid transport rates. In conventional particulate materials, diffusional limitations may be a major concern, which may result in poor transport rates. Accordingly, there has been significant activity in the development of novel resin materials to overcome this limitation (1, 2).

Currently, there is a plethora of stationary phase materials available to the chromatographic practitioner. Thus, it becomes necessary to compare the various resins and evaluate their efficacy for preparative modes of chromatography. There have been several reports in the literature comparing different types of resin materials.

- Boschetti, 1994 (3) compared the variation of the dynamic binding capacity as a function of the flow rate for a variety of commercial ion-exchange resins.
- Horvath et al., 1994 (4) characterized POROS, Hyper-D, and Mono materials by measuring their dynamic capacity, reduced plate heights, protein recovery, and resolution factors for a mixture of six model proteins. However, the separation of the proteins was carried out under linear adsorption conditions.
- Levison et al., 1996 (5) compared the effect of flow rate on the performance of Whatman Express-Ion Exchanger Q and Pharmacia Q-Sepharose Fast Flow. The comparison was based on dynamic capacity measurements and linear gradient separation of egg-white feedstock. However, no attempt was made to optimize the gradient conditions and the same gradient was employed on both the resins.
- In a more wide-ranging study, Levison et al., 1997 (6) compared over 70 commercial ion-exchange media. The comparison was based on physical tests such as swelling and packing density and functional tests such as protein capacity and resolution under identical linear gradient conditions. The data resulting from this study was "descriptive, rather than prescriptive" and underlined the need for extensive media screening.
- Recently, Nash and Chase, 1998 (7) compared diffusion and diffusion–convection matrices for ion-exchange separations. The authors in this study employed pressure drop measurements, plate height measurements, dynamic capacity measurements, protein recovery measurements and resolution of a mixture of two model proteins to characterize the various matrices. While the analysis of the plate height measurements resulted in a comparison of pore diffusional parameters, it neglected contributions from surface diffusion and adsorption-desorption kinetics.

In order to model preparative separations, it is necessary to have appropriate isotherm and transport models. The steric mass action (SMA) formalism (8) has been demonstrated to accurately describe protein binding in non-

linear ion-exchange systems. This isotherm has been employed in concert with the equilibrium-dispersive model to accurately describe chromatographic behavior in isocratic (9), linear gradient (10), and step-gradient systems (11). To choose an appropriate transport model, one needs information on the relative rates of the various transport mechanisms in a given stationary phase material. This can be achieved through the comparison of appropriate dimensionless groups. Wang and coworkers (12–15) employed such an analysis to identify appropriate transport models (12) and to study the effect of various rate-controlling mechanisms on the chromatographic behavior of solutes (13–15).

To construct these dimensionless groups, one needs to estimate the various rate parameters for a given resin material. Pulse analysis has been widely employed in the literature to estimate these rate parameters (16, 17). To derive the rate parameters from pulse injections, one needs to have equations relating HETP to operational parameters. Van Deemter et al., 1956 (18) were among the first to derive the dependence of the HETP on the flow velocity. Giddings, 1965 (19) modified van Deemter's equation to reflect the coupling of eddy diffusion and film mass transport. A more comprehensive treatment of the effect of the various rate parameters on the overall HETP and a methodology to estimate the individual plate height contributions has been provided by Horvath and Lin, 1978 (20). However, in these studies the authors do not include the effects of surface diffusion. Knox and Scott, 1983 (21) included surface diffusion and studied the effect of retention on the $B$ and $C$ terms in the van Deemter equation in reversed phase systems. With the relatively recent advent of gigaporous particles that allow intraparticle convection, the HETP equations have been suitably modified (22–24).

Pulse injections under retained and unretained conditions are employed in this article to estimate the transport properties for different types of stationary phase materials. Dimensionless groups are then constructed to evaluate the relative contributions of the various transport mechanisms. This analysis is then used to determine the rate model for a given resin material. Finally, this model is employed in concert with the steric mass action (SMA) isotherm to model displacement separations.

## THEORY

### Steric Mass Action Formalism

SMA formalism (8) is a three-parameter model for the description of multicomponent protein–salt equilibrium in ion-exchange systems. The multipointed binding of the protein molecule to the stationary phase is represented as a stoichiometric exchange of mobile phase protein and bound counterions

as follows:

$$C_i + \nu_i \overline{Q}_1 \Leftrightarrow Q_i + \nu_i C_1 \tag{1}$$

where $\nu_i$ is the characteristic charge of the protein, the subscript "1" represents the salt counterion, and $\overline{Q}_1$ is the number of sites on the stationary phase available for exchange with the protein. The equilibrium constant for the above reaction is given by

$$K_{SMA} = \left(\frac{Q_i}{C_i}\right)\left(\frac{C_1}{Q_1}\right)^{\nu_i} \tag{2}$$

In addition to binding to $\nu_i$ sites, each adsorbed protein molecule will also sterically shield $\sigma_i$ counterions on the stationary phase. The number of counterions blocked by a particular protein will be proportional to the concentration of the protein on the adsorptive surface (25):

$$\hat{Q}_i = \sigma_i Q_i \tag{3}$$

The steric factor $\sigma_i$ describes the nonlinear adsorption behavior of the proteins. On the other hand, the equilibrium constant $K$ and the characteristic charge $\nu$ describe the linear adsorption behavior of the proteins.

An ion-exchange surface must maintain electroneutrality. This is given by the following equation for a multicomponent mixture:

$$\Lambda = \overline{Q}_1 + \sum_{i=2}^{NC} (\nu_i + \sigma_i) Q_i \tag{4}$$

Equations (2)–(4) constitute the SMA formalism.

## Mass Transport Equations

The most complete transport model that can describe the chromatographic behavior of solutes is the general rate model. However, it is very expensive computationally. Thus, employing it for optimization of preparative chromatography would be impractical. As far as possible, one would like to employ lumped rate models such as the transport-dispersive and reaction-dispersive models described below. Analysis of the various dimensionless groups enables one to decide which lumped rate model to employ for a given resin system.

In this article the following lumped rate models (26) were considered.

### *A) Transport-Dispersive Model*

$$\frac{\partial C_i}{\partial \tau} + \beta \frac{\partial Q_i}{\partial \tau} + \frac{\partial C_i}{\partial x} = \frac{1}{\mathrm{Pe}_i} \frac{\partial^2 C_i}{\partial x^2} \tag{5}$$

$$\frac{\partial Q_i}{\partial \tau} = \mathrm{St}_i (Q_i^{\mathrm{equil}} - Q) \tag{6}$$





MARCEL DEKKER, INC.
270 Madison Avenue, New York, New York 10016

The symbols are defined in the Nomenclature section. In this model the Peclet number, $Pe_a$, accounts for axial dispersion effects whereas the Stanton number, St, represents a lumped mass transport coefficient that accounts for film, pore, and/or surface diffusion effects (depending on the relative importance of these phenomena).

### B) Reaction-Dispersive Model

$$\frac{\partial C_i}{\partial \tau} + \beta \frac{\partial Q_i}{\partial \tau} + \frac{\partial C_i}{\partial x} = \frac{1}{\mathrm{Pe}_i} \frac{\partial^2 C_i}{\partial x^2} \tag{7}$$

$$\frac{\partial Q_i}{\partial \tau} = k_{\mathrm{ads}} C_i \overline{Q}_1^{\nu} - k_{\mathrm{des}} C_1^{\nu} Q_i \tag{8}$$

Equation (8) has been written for the SMA formalism. This rate model can be employed when the kinetics of adsorption–desorption is the rate limiting resistance.



## Pulse Analysis

In this article the dependence of HETP on two operational parameters (flow rate and salt concentration) has been analyzed to estimate the appropriate rate parameters for protein separations in ion-exchange systems. The general rate model in conjunction with the SMA formalism under linear adsorption conditions was transformed into the Laplace domain. Subsequently, the HETP equations were derived using the first and second moments of the solution in the Laplace domain. The following equations relate the effect of flow rate and the salt concentration on the HETP of protein pulses in ion-exchange systems:

$$H = \frac{2D_{\mathrm{a}}}{Lu} + \frac{2(1-\varepsilon_{\mathrm{i}})\varepsilon_{\mathrm{p}} b_0^2 u}{[\varepsilon_{\mathrm{i}} + (1-\varepsilon_{\mathrm{i}})\varepsilon_{\mathrm{p}} b_0]^2} \times \left[ \frac{R}{3k_{\mathrm{f}}} + \frac{R^2}{15 D_{\mathrm{p}}(1 + [b_0 - 1]r)} + \frac{b_0 - 1}{b_0^2 k'_{\mathrm{des}}} \right] \tag{9}$$

$$k' = \frac{1-\varepsilon_{\mathrm{p}}}{\varepsilon_{\mathrm{p}}} K_{\mathrm{SMA}} \left( \frac{\Lambda}{C_{\mathrm{salt}}} \right)^{\nu} \tag{10}$$

$$b_0 = 1 + k' \tag{11}$$

$$r = D_{\mathrm{p}}/D_{\mathrm{s}} \tag{12}$$

Now, in the SMA formalism,

$$k'_{\mathrm{des}} = k_{\mathrm{des}} C_{\mathrm{salt}}^{\nu} \tag{13}$$



MARCEL DEKKER, INC.
270 Madison Avenue, New York, New York 10016

Hence, substituting for $C_{salt}$ using Eqs. (10) and (11):

$$H = \frac{2D_a}{Lu} + \frac{2(1-\varepsilon_i)\varepsilon_p b_0^2 u}{[\varepsilon_i + (1-\varepsilon_i)\varepsilon_p b_0]^2} \times \left[\frac{R}{3k_f} + \frac{R^2}{15D_p(1+[b_0-1]r)} + \frac{(b_0-1)^2}{b_0^2 k''_{des}}\right] \quad (14)$$

where

$$k''_{des} = \frac{1-\varepsilon_p}{\varepsilon_p} K_{SMA}\Lambda^{\nu} k_{des} \quad (15)$$

The various symbols are defined in the Nomenclature section. The operational parameters are $u$ (the linear velocity) and $b_0$, which is related to the retention factor. For the SMA isotherm the dependence of the retention factor, $k'$, on the salt concentration is illustrated in Eq. (10). As can be seen in Eqs. (9)–(15), there are five rate parameters to be estimated: the axial dispersion parameter, $D_a$; the film mass transfer coefficient, $k_f$; the pore diffusion coefficient, $D_p$; the surface diffusion coefficient, $D_s$; and the desorption constant, $k_{des}$.

Now, the axial dispersion parameter, $D_a$, can be divided into contributions from molecular diffusion and eddy diffusion. For macromolecular systems the contributions from molecular diffusion are usually negligible (16). Hence the axial dispersion parameter can be defined as follows:

$$D_a = \zeta u \quad (16)$$

where $\zeta$ is a proportionality factor. Hence, Eq. (14) becomes

$$H = \frac{2\zeta}{L} + \frac{2(1-\varepsilon_i)\varepsilon_p b_0^2 u}{[\varepsilon_i + (1-\varepsilon_i)\varepsilon_p b_0]^2} \times \left[\frac{R}{3k_f} + \frac{R^2}{15D_p(1+[b_0-1]r)} + \frac{(b_0-1)^2}{b_0^2 k''_{des}}\right] \quad (17)$$

Under unretained conditions, $b_0 = 1$ and hence,

$$H = \frac{2\zeta}{L} + \frac{2(1-\varepsilon_i)\varepsilon_p u}{[\varepsilon_i + (1-\varepsilon_i)\varepsilon_p]^2}\left[\frac{R}{3k_f} + \frac{R^2}{15D_p}\right] \quad (18)$$

The film mass transfer coefficient, $k_f$, is estimated using the well-established correlation (27):

$$Sh = 2 + 1.45Re^{1/2}Sc^{1/3} \quad (19)$$

In addition to rate processes, external sources may also contribute to the overall HETP. Thus, for an accurate determination of rate parameters, one needs





MARCEL DEKKER, INC.
270 Madison Avenue, New York, New York 10016

to account for the contribution from extracolumn sources. The HETP contributions from extracolumn band-broadening are computed as follows:

$$H_{ec} = L\left[\frac{\sigma_{ec}F}{V_0 b_0}\right]^2 \tag{20}$$

## EXPERIMENTAL METHODS

### Materials

Sodium monobasic phosphate, sodium dibasic phosphate, sodium nitrate, α-chymotrypsinogen A, ribonuclease A, neomycin sulfate, and blue dextran were purchased from Sigma Chemical (St. Louis, MO). Sodium chloride was purchased from Aldrich Chemical (Milwaukee, WI). Two strong cation-exchange columns were packed with Waters SP stationary phase material (sulfopropyl, 40 μm) and Amersham Pharmacia Biotech's HP Sepharose resin (sulfopropyl, 34 μm). The FF Sepharose column was obtained prepacked from Amersham Pharmacia Biotech. The POROS R/H reversed phase column (0.46 i.d. × 5 cm) was obtained from PerSeptive Biosystems (Framingham, MA).

### Apparatus

Pulse injections were made using a WISP model 712 autoinjector (Waters Corporation, Milford, MA) connected to a model 650E Advanced Protein Purification system (Waters Corporation, Milford, MA) with a model 484 Tunable Absorbance Detector (Waters Corporation, Milford, MA). Data acquisition and processing were carried out using a Millenium 2010 chromatography workstation (Waters Corporation, Milford, MA). Sodium nitrate was monitored at 310 nm while the proteins were monitored at 254 nm.

All displacement experiments were carried out using a Model 590 programmable HPLC pump (Waters Corporation, Milford, MA) connected to the chromatographic columns via a Model C10W 10-port valve (Valco, Houston, TX). Data acquisition and processing were carried out using a Millenium 2010 chromatography workstation (Waters Corporation, Milford, MA). Fractions of the column effluent were collected using a LKB 2212 Helirac fraction collector (LKB, Sweden). Protein and displacer analysis for the collected fractions were carried out using a WISP model 712 autoinjector (Waters Corporation, Milford, MA) connected to a model 650E Advanced Protein Purification system (Waters Corporation, Milford, MA) with a model 484 Tunable Absorbance Detector (Waters Corporation, Milford, MA). UV absorbance of samples was measured on a Lambda 6 UV-Vis spectrophotometer (Perkin-Elmer).

## Procedures

### Estimation of Extracolumn Contributions

Pulse injections of the solutes were made at various flow rates with the column off-line to estimate extracolumn contributions from the chromatography system itself. The first and second moments of the resultant peaks were computed.

### Estimation of Porosities

The interstitial and particle porosities were obtained from unretained data. Pulse injections of solutes were made at high salt concentration (1 M). Under these conditions, the proteins used in this study were unretained in all the stationary phase materials. This was verified by comparing their elution volumes with that of a small molecule such as sodium nitrate.

The following equation relates the first moment of a given peak to the flow velocity:

$$\mu_1 = \frac{L}{u}(\varepsilon_i + (1 - \varepsilon_i)\varepsilon_p b_0) \tag{21}$$

where $\mu_1$ is the first moment of the elution peak. Under unretained conditions, the value of $b_0$ (described above in Eq. 11) is 1. Pulse injections of blue dextran (average MW 2,000,000) were made under unretained conditions. It was assumed that these bulky solutes could only access the interstitial volumes and were excluded from the pores. Thus, the interstitial porosities were estimated from the first moments of their peaks. Having determined the interstitial porosity, the particle porosities of the various solutes employed in this study were estimated from the first moments of their unretained peaks using Eq. (21).

### Estimation of HETP

Pulse injections were made under various combinations of salt concentrations and superficial velocities. Pulse injections were made at several different superficial velocities at a given salt concentration. This was repeated for several salt concentrations. The first moments of the resultant peaks were employed to estimate the $b_0$ for a given salt concentration using Eq. (21).

The HETP of the resultant elution peaks were computed as follows: Gaussian peaks were fitted to the elution profiles and the HETP of the fitted Gaussian peaks were calculated using the following equation:

$$H = \frac{L}{5.54}\left(\frac{t_{w,0.5}}{t_r}\right)^2 \tag{22}$$





MARCEL DEKKER, INC.
270 Madison Avenue, New York, New York 10016

Figure 1 illustrates this technique. The raw data were exported from the Millenium 2010 workstation and fitted with a Gaussian profile using MATLAB's constrained optimization routine, CONSTR. As can be seen in the figure, the peaks are well fit by the Gaussian profiles, justifying the use of this technique. Furthermore, this methodology eliminates the errors that enter into the calculation of the second moments because of instrument noise.

The HETP computed using Eq. (22) is the total HETP, $H_{tot}$, of the system. To obtain the HETP of the column alone, $H_{col}$, the extracolumn contribution (computed using Eq. 20) was subtracted from $H_{tot}$:

$$H_{col} = H_{tot} - H_{ec} \tag{23}$$

Following this, the HETP due to film mass transport, $H_{film}$, was computed using the correlation described in Eq. (19) and subtracted to yield the following:

$$H'_{col} = H_{col} - H_{film} \tag{24}$$

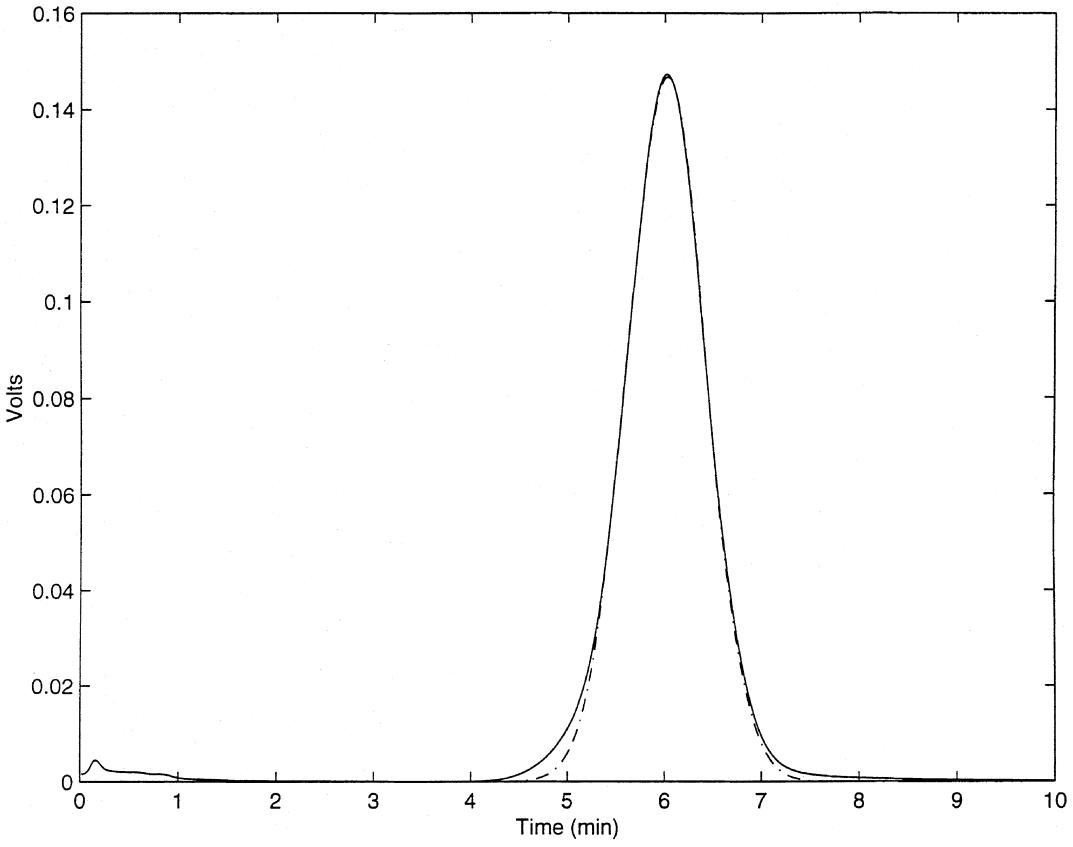


FIG. 1 Gaussian fit to experimental peak profile. Solid line: UV trace of protein peak. Dashed line: Gaussian fit to UV trace.





MARCEL DEKKER, INC.
270 Madison Avenue, New York, New York 10016

where $H'_{col}$ represents the HETP of the column without the film mass transfer contribution. (Note: This is done to facilitate parameter estimation.)

$H'_{col}$ was then plotted as a function of velocity at various salt concentrations. The MATLAB function, CONSTR, was employed to fit the data using Eq. (18). This enabled the estimation of the axial dispersion parameter and the pore diffusivity.

From Eq. (17), the slope, $S$, of the $H'_{col}$ vs $u$ plot is expected to vary with $b_0$ as

$$S = \frac{2(1 - \varepsilon_i)\varepsilon_p b_0^2}{[\varepsilon_i + (1 - \varepsilon_i)\varepsilon_p b_0]^2}\left[\frac{R^2}{15D_p(1 + (b_0 - 1)r)} + \frac{(b_0 - 1)^2}{b_0^2 k''_{des}}\right] \quad (25)$$

Thus, by evaluating the slope, $S$, at the various salt concentrations, Eq. (25) can be readily employed to estimate $r$ and $k''_{des}$. Once again, the MATLAB function, CONSTR, was employed to carry out the necessary fit of the data.



### Estimation of SMA Parameters of Proteins

The linear SMA parameters of the proteins ($K$ and $\nu$) were determined using the protocols outlined by Gadam et al., 1993 (28). Briefly, the characteristic charge and the equilibrium constant were determined using linear elution retention data at different mobile phase salt concentrations. The steric factor, σ, was obtained from a frontal experiment carried out at a low salt concentration (<100 mM $Na^+$) at a low flow rate. The resulting SMA parameters of the two proteins employed in this study (α-chymotrypsinogen A and ribonuclease A) are given in Tables 1a and 1b.

TABLE 1a
SMA Parameters for α-Chymotrypsinogen A

| Resin | $\nu$ | $K$ | σ |
|---|---|---|---|
| 40 μm Waters | 4.8 ± 0.17 | 0.0066 | 52 |
| HP Sepharose | 4.67 ± 0.08 | 0.0025 | 10 |
| FF Sepharose | 4.44 ± 0.1 | 0.0039 | 10 |

TABLE 1b
SMA Parameters for Ribonuclease A

| Resin | $\nu$ | $K$ | σ |
|---|---|---|---|
| 40 μm Waters | 4.2 ± 0.18 | 0.0061 | 40 |
| HP Sepharose | 3.84 ± 0.08 | 0.007 | 10 |
| FF Sepharose | 3.71 ± 0.7 | 0.0077 | 12 |



MARCEL DEKKER, INC.
270 Madison Avenue, New York, New York 10016

### Estimation of SMA Parameters of Displacer

The characteristic charge of the displacer was determined from the induced salt gradient produced from passing a front of the displacer at a known concentration. The equilibrium constant and the steric factor were then determined by a best fit of the adsorption isotherms of the displacer obtained at various mobile phase salt concentrations (29).

### Estimation of the Mass Transport Properties of the Displacer

The lumped mass transfer parameter of the displacer was obtained by a least-squares fit of the breakthrough curves of the displacer at two different flow rates (30). The concentrations of the displacer and the salt in these frontal runs were the same as those employed in the subsequent displacement experiments.



### Displacement Experiments

The column was initially equilibrated with the carrier and subsequently perfused with feed, displacer, and regenerant solutions. The feed load, salt concentration, and displacer concentration employed for the separation are given in the figure legends of the respective chromatograms. 500 μL fractions were collected for subsequent analysis of protein and displacer concentration in the effluent.

### Protein Analysis

Analysis of the fractions collected during the displacement experiments was performed on a POROS R/H reversed phase HPLC under gradient conditions. The fractions were diluted 1–10 fold. The mobile phases employed for the analyses were deionized water (A) and 90% ACN (v/v) in deionized water adjusted to pH 2.2 with TFA (B). A 20-minute gradient from 0 to 100% B was employed for the analysis of α-chymotrypsinogen A and ribonuclease A. The proteins were detected using a UV-VIS detector at 254 nm.

### Displacer Analysis

Neomycin sulfate was analyzed using a phenol-sulfuric acid assay (31). The fractions were diluted 5–20 fold. 0.8 mL of the sample was mixed with 3.2 mL of sulfuric acid, reacted for 1 minute, and cooled to room temperature. 50 μL of 90% phenol (w/v) was then added, and the resultant mixture was allowed to equilibrate for 30 minutes. The absorbance was read at 480 nm.



MARCEL DEKKER, INC.
270 Madison Avenue, New York, New York 10016

TABLE 2
Resins Employed in This Study

| Resin | Particle size (μm) | Column dimensions (cm × cm) | Ionic capacity (mM) |
|---|---|---|---|
| Waters | 40 | 1 × 8 | 525 |
| HP Sepharose | 34 | 1 × 9 | 1200 |
| FF Sepharose | 90 | 1.6 × 10.5 | 1200 |

## RESULTS AND DISCUSSION

The various resins employed in this study are listed in Table 2. The Waters resin possesses a polymethacrylate backbone while the Pharmacia resins possess a crosslinked agarose backbone. As can be seen in Table 2, there is a considerable difference in the ionic capacities of these resins. The ionic capacities listed in Table 2 are based on the solid stationary phase volume. However, the ionic capacities suggested by the manufacturers are usually given in terms of column volume. Thus, the capacities listed in Table 2 were recomputed on a per column volume basis to effect a comparison with manufacturer's values. It turns out that the capacities listed in Table 2 are in reasonable agreement with manufacturer's suggested values. The suggested ionic capacities for both the sepharose resins are in the 0.18–0.25 mmol/mL column volume range whereas the capacities listed in Table 2 translate to 0.22 (HP Sepharose) and 0.26 (FF Sepharose) mmol/mL column volume, respectively. On the other hand, for the Waters resin, the ionic capacity listed in Table 2 translates to 0.16 mmol/mL column volume which is in good agreement with the suggested nominal ligand density of 0.2 mmol/mL.

Two model proteins (α-chymotrypsinogen A and ribonuclease A) were employed in this article to illustrate the resin characterization methodology. The porosities of the proteins on the various resins are tabulated in Tables 3a and

TABLE 3a
Interstitial and Particle Porosities of α-Chymotrypsinogen A on the Various Resins

| Resin | Interstitial porosity | Particle porosity | Total porosity |
|---|---|---|---|
| 40 μm Waters | 0.37 ± 0.009 | 0.51 ± 0.009 | 0.69 ± 0.006 |
| HP Sepharose | 0.32 ± 0.004 | 0.73 ± 0.014 | 0.82 ± 0.01 |
| FF Sepharose | 0.31 ± 0.006 | 0.68 ± 0.006 | 0.78 ± 0.004 |





MARCEL DEKKER, INC.
270 Madison Avenue, New York, New York 10016

TABLE 3b
Interstitial and Particle Porosities of Ribonuclease A on the Various Resins

| Resin | Interstitial porosity | Particle porosity | Total porosity |
|---|---|---|---|
| 40 μm Waters | 0.37 ± 0.009 | 0.54 ± 0.01 | 0.71 ± 0.01 |
| HP Sepharose | 0.32 ± 0.004 | 0.77 ± 0.008 | 0.84 ± 0.006 |
| FF Sepharose | 0.31 ± 0.006 | 0.8 ± 0.03 | 0.71 ± 0.02 |

3b. The sepharose resins possess the lowest interstitial porosities. On the other hand, the particle porosities are higher in the sepharose materials. (Note: This may partially account for the higher ionic capacities observed with the sepharose resins as the ionic capacity is evaluated per liter of solid stationary phase material.)

The variation of the HETP of the proteins as a function of the linear velocity under unretained conditions is illustrated in Figs. 2a–b. As is evident from the figures, the dependence of the HETP on velocity is linear on both the poly-

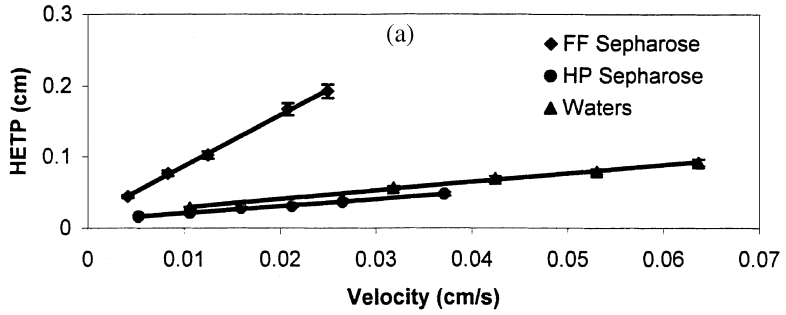


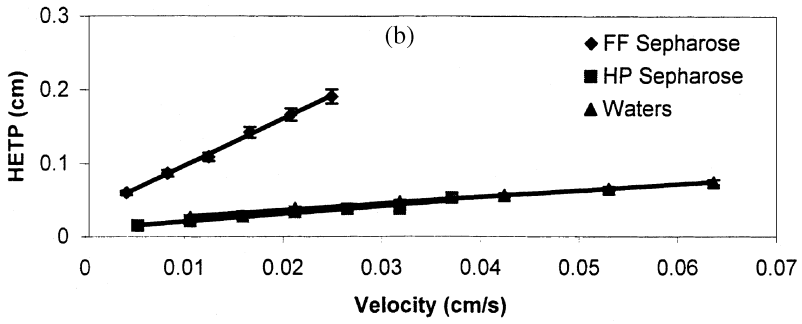


FIG. 2 HETP plots on the three resins under unretained conditions. Mobile phase: 1 M NaCl in 50 mM phosphate buffer (pH 6). (a) α-Chymotrypsinogen A. (b) Ribonuclease A.





MARCEL DEKKER, INC.
270 Madison Avenue, New York, New York 10016

TABLE 4a
Summary of Unretained Results for α-Chymotrypsinogen A

| Resin | Slope of HETP plot | $D_p$ (cm$^2$/s)[a] | ζ (cm)[b] | $\tau_{tor}$ |
|---|---|---|---|---|
| 40 μm Waters | 1.2 ± 0.04 | 3.0e-7 | 1.7e-2 ± 0.002 | 1.5 |
| HP Sepharose | 0.97 ± 0.03 | 3.0e-7 | 1.0e-2 ± 0.001 | 2.2 |
| FF Sepharose | 7.22 ± 0.15 | 2.9e-7 | 1.5e-2 ± 0.002 | 2.1 |

[a] Obtained from the slope of the HETP plot.
[b] Obtained from the *y* intercept of the HETP plot.

TABLE 4b
Summary of Unretained Results for Ribonuclease A

| Resin | Slope of HETP plot | $D_p$ (cm$^2$/s)[a] | ζ (cm)[b] | $\tau_{tor}$ |
|---|---|---|---|---|
| 40 μm Waters | 0.88 ± 0.02 | 4.1e-7 | 1.8e-2 ± 0.001 | 1.6 |
| HP Sepharose | 1.04 ± 0.11 | 2.7e-7 | 1.0e-2 ± 0.0025 | 3.3 |
| FF Sepharose | 6.4 ± 0.15 | 3.2e-7 | 3.3e-2 ± 0.002 | 2.6 |

[a] Obtained from the slope of the HETP plot.
[b] Obtained from the *y* intercept of the HETP plot.



methacrylate and the sepharose resins. In fact, the HETPs on the HP Sepharose resin are almost identical to those on the Waters material for both the proteins under unretained conditions. This is not surprising since their particle sizes are similar (Table 2). As expected, the HETPs on the FF Sepharose resin are significantly higher due to the larger particle size of this material. Using these plots, the axial dispersion parameter, ζ, and the pore diffusivity, $D_p$, were computed using Eq. (18). Tables 4a and 4b list these parameters for the various resins. In a packed bed the pore diffusivity is related to the molecular diffusivity as follows (32):

$$D_p = \frac{\varepsilon_p D_m}{\tau_{tor}} \tag{26}$$

where $\tau_{tor}$ is the tortuosity factor. The tortuosity factors computed using Eq. (26) are also shown in Tables 4a and 4b. The molecular diffusivities, $D_m$, of the proteins were obtained from Tyn and Gusek, 1990 (33). As can be seen in Table 4, the tortuosity factors of the sepharose resins range from 2.1 to 3.3. This value is within the 2 to 6 range normally expected for particulate resins. On the other hand, for the 40 μm Waters resin the tortuosity factor is approximately 1.5.

Figures 3(a–f) present the HETP plots of the model proteins at various salt concentrations on the various resins. (Note: Only three of the salt concentrations are shown in these figures for purposes of clarity.) As is evident from the



MARCEL DEKKER, INC.
270 Madison Avenue, New York, New York 10016

figures, the slopes of the HETP plots vary with the salt concentration. The solid lines in these figures are least-square fits to the data. According to Eq. (17), the axial dispersion term, $2\zeta/L$, is not expected to be a function of $b_0$. Thus, the straight line fits in Figs. 3(a–f) were made after fixing the $y$-intercept

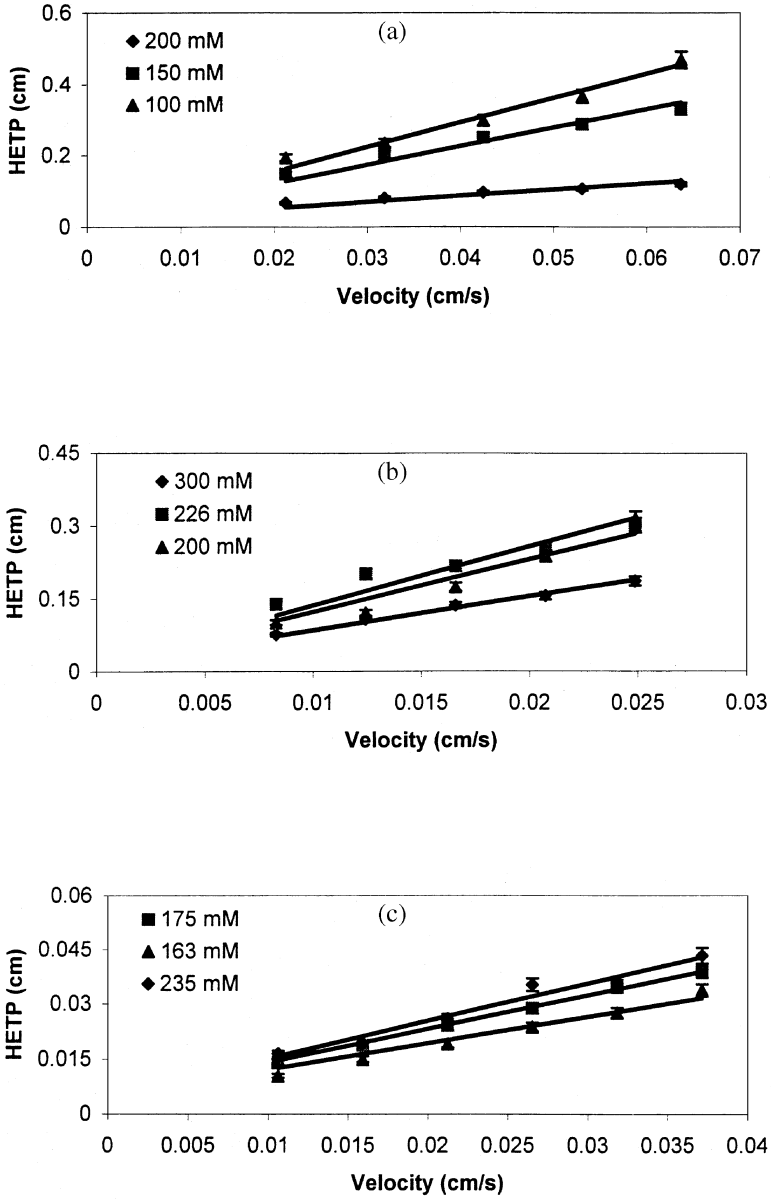


FIG. 3 HETP plots at various salt concentrations on the three resins. Solid lines are least squares fits to the data points. (a) α-Chymotrypsinogen A on the Waters resin. (b) α-Chymotrypsinogen A on the HP Sepharose resin. (c) α-Chymotrypsinogen A on the FF Sepharose resin. (d) Ribonuclease A on the Waters resin. (e) Ribonuclease A on the HP Sepharose resin. (f) Ribonuclease A on the FF Sepharose resin. (Note: the total salt concentrations are indicated directly on the figure).

(continued)





MARCEL DEKKER, INC.
270 Madison Avenue, New York, New York 10016

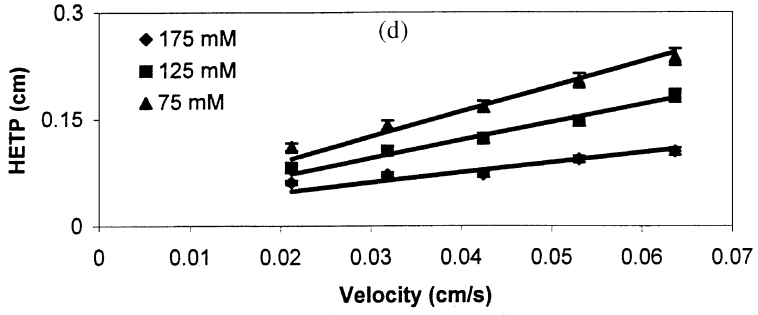


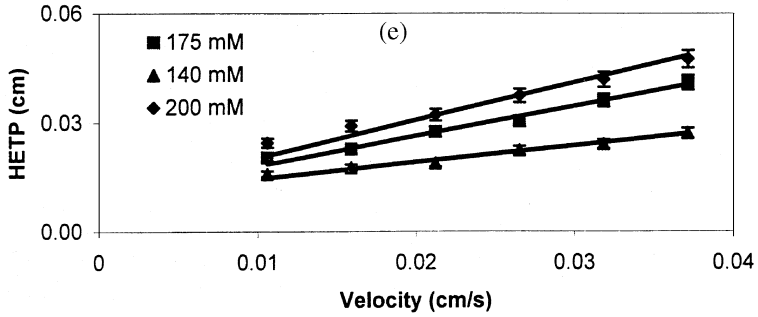


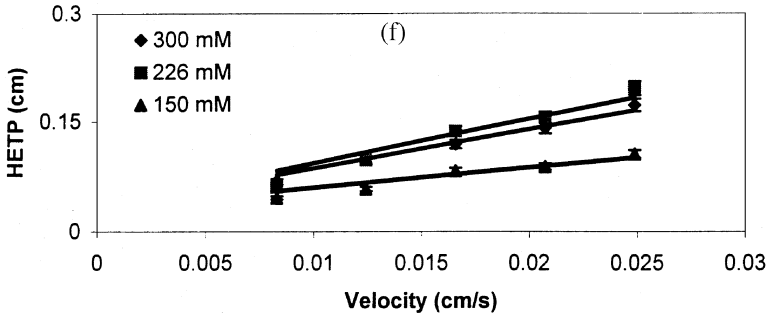


FIG. 3 Continued

at the value obtained from the unretained results (Fig. 2). As can be seen in Fig. 3, this assumption resulted in good fits of the data.

In order to determine $r$ and $k''_{des}$, the slope of the HETP curves ($S$) was plotted as a function of $b_0$ (Figs. 4a–f). The solid lines in these figures are the best-fit curves of the data using Eq. (25). The $r$ and $k''_{des}$ obtained for the two proteins on the various resins are presented in Table 5a and b. It turns out that the ratio of pore to surface diffusion, $r$, has a significant effect on the shape of the $S$ vs $b_0$ curve (Fig. 4). When $r = 0$ (Fig. 4a), i.e., when

surface diffusion is negligible or absent, the curve monotonically increases and then flattens out. On the other hand, for finite values of $r$ (e.g., $r = 0.1$, Fig. 4b), when surface diffusion can be significant, there is a distinct maxima in the curve. Hence, the shape of the $S$ vs $b_0$ curve can provide

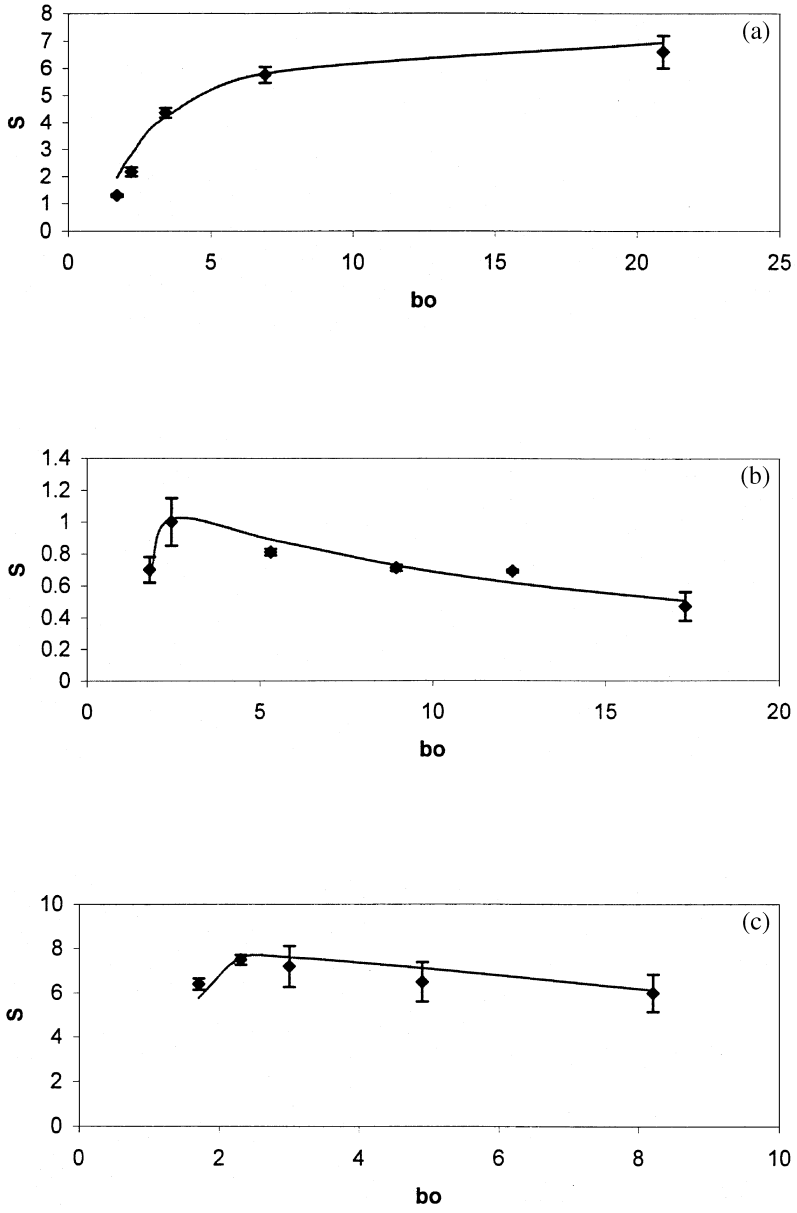


FIG. 4 Variation of the slope of the HETP plots as a function of $b_0$ on the three resins. Solid lines are least squares fits to the data points. (a) α-Chymotrypsinogen A on the Waters resin. (b) α-Chymotrypsinogen A on the HP Sepharose resin. (c) α-Chymotrypsinogen A on the FF Sepharose resin. (d) Ribonuclease A on the Waters resin. (e) Ribonuclease A on the HP Sepharose resin. (f) Ribonuclease A on the FF Sepharose resin.

(continued)





MARCEL DEKKER, INC.
270 Madison Avenue, New York, New York 10016

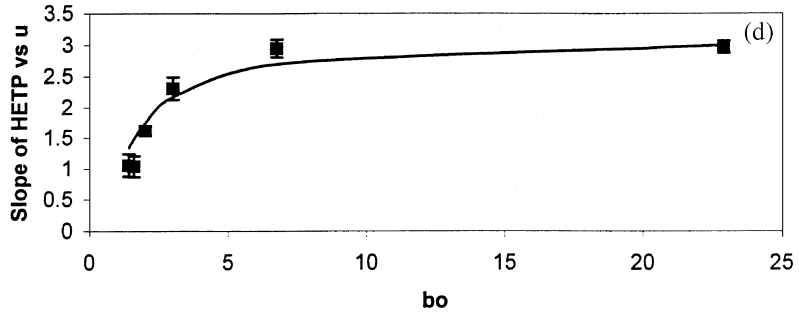


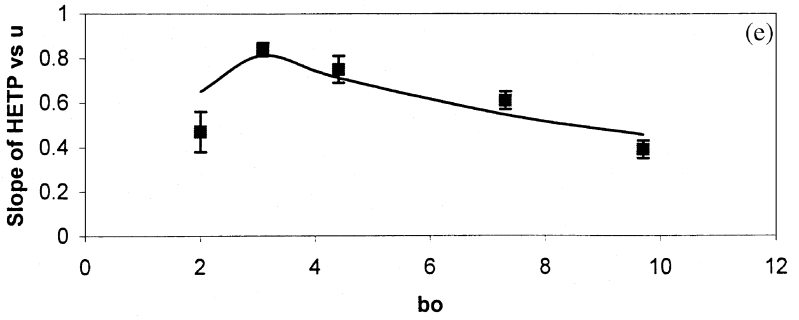


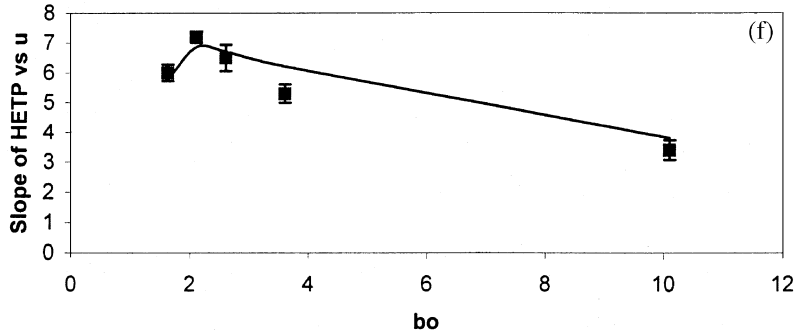


FIG. 4 Continued

significant insight into the importance of surface diffusion for a given resin material.

As seen in Figs. 4(a–f), there is a qualitative difference in the shape of these curves on the sepharose and polymethacrylate materials. A distinct maxima was observed on the sepharose resins for both proteins, in contrast to the polymethacrylate resin. This strongly suggests that surface diffusion may play an important role in the sepharose resins.





MARCEL DEKKER, INC.
270 Madison Avenue, New York, New York 10016

TABLE 5a
Summary of Results for Injections of α-Chymotrypsinogen A Made under Retained Conditions

| Resin | $r^a$ | $D_s$ (cm$^2$/s)$^b$ | $k''_{des}$ (s$^{-1}$)$^a$ | $k_{des}$ (mM$^{-\nu}$·s$^{-1}$)$^c$ |
|---|---|---|---|---|
| 40 μm Waters | 0 | No surface diffusion | 8,000 ± 310 | 1.1e-7 |
| HP Sepharose | 0.1 ± 0.05 | 3e-8 | 12,000 ± 250 | 1.0e-7 |
| FF Sepharose | 0.05 ± 0.07 | 1.45e-8 | 11,000 ± 29 | 1.5e-7 |

[a] Obtained by fitting curves in Figs. 4(a–c).
[b] Obtained using Eq. (12).
[c] Obtained using Eq. (15).

TABLE 5b
Summary of Results for Injections of Ribonuclease A Made under Retained Conditions

| Resin | $r^a$ | $D_s$ (cm$^2$/s)$^b$ | $k''_{des}$ (s$^{-1}$)$^a$ | $k_{des}$ (mM$^{-\nu}$·s$^{-1}$)$^c$ |
|---|---|---|---|---|
| 40 μm Waters | 0 | No surface diffusion | 6000 ± 241 | 4.4e-6 |
| HP Sepharose | 0.2 ± 0.07 | 5.4e-8 | 4200 ± 125 | 3e-6 |
| FF Sepharose | 0.15 ± 0.09 | 4.85e-8 | 3000 ± 137 | 5.4e-6 |

[a] Obtained by fitting curves in Figs. 4(d–f).
[b] Obtained using Eq. (12).
[c] Obtained using Eq. (15).



Having estimated the various parameters, several dimensionless groups were determined to ascertain the relative importance of the various transport mechanisms. Tables 6a–c list the dimensionless groups employed in this study and their values for the various resins. The dimensionless groups relate the rates of the various transport mechanisms to the convective transport rate. The values of the dimensionless groups defined in Table 6a are listed in Tables 6b and 6c. The dimensionless groups have the linear velocity in the data (with the exception of $N_{Pe}$) to enable direct comparison of the relative values of these dimensionless groups at any velocity. As seen, the value of $N_{Pe}$ is an order of magnitude higher than the limiting dimensionless groups in all cases. As seen in Table 6a, the values of $N_s$ and $N_{des}$ are dependent on the salt concentration. Surface diffusion and desorption kinetic limitations are more pronounced at lower salt concentrations. Accordingly, a relatively low salt concentration of 50 mM was employed for these calculations. As can be seen from Tables 6b and 6c, pore diffusion seems to be the dominant transport mechanism on the polymethacrylate resin. On the other hand, both pore and surface diffusion appear to be important on the sepharose resins. The reason for this behavior may be due to the fact that the capacities of the sepharose resins are higher than those of the polymethacrylate resins. This is consistent with the observations

TABLE 6a
Dimensionless Groups Employed in This Article

| Dimensionless groups | Description |
|---|---|
| $N_p = \frac{D_p L}{R^2 u}$ | $\frac{\text{Pore diffusion}}{\text{Convection}}$ |
| $N_s = \left(\frac{1-\varepsilon_p}{\varepsilon_p}\right)\frac{D_s L}{R^2 u} K_{SMA}\left(\frac{\bar{Q}_1}{C_{salt}}\right)^{\nu}$ | $\frac{\text{Surface diffusion}}{\text{Convection}}$ |
| $N_{des} = \frac{k_{des} C_{salt}^{\nu} L}{u}$ | $\frac{\text{Desorption kinetics}}{\text{Convection}}$ |
| $N_f = \frac{3k_f L}{Ru}$ | $\frac{\text{Film transport}}{\text{Convection}}$ |
| $\frac{1}{N_{Pe}} = \frac{D_a}{Lu}$ | $\frac{\text{Axial dispersion}}{\text{Convection}}$ |

TABLE 6b
Dimensionless Groups for α-Chymotrypsinogen A

| Resin | $N_p$ | $N_s$[a] | $N_{Pe}$ | $N_f$ | $N_{des}$[a] |
|---|---|---|---|---|---|
| 40 μm Waters | 0.6/u | No surface diffusion | 471 | 47/u | 126/u |
| HP Sepharose | 0.9/u | 3.5/u | 900 | 16/u | 77/u |
| FF Sepharose | 0.15/u | 0.56/u | 700 | 5/u | 55/u |

[a] Evaluated at a $Na^+$ concentration of 50 mM.

TABLE 6c
Dimensionless Groups for Ribonuclease A

| Resin | $N_p$ | $N_s$[a] | $N_{Pe}$ | $N_f$ | $N_{des}$[a] |
|---|---|---|---|---|---|
| 40 μm Waters | 1/u | No surface diffusion | 444 | 54/u | 481/u |
| HP Sepharose | 0.84/u | 6.0/u | 900 | 24/u | 90/u |
| FF Sepharose | 0.14/u | 0.85/u | 303 | 5/u | 114/u |

[a] Evaluated at a $Na^+$ concentration of 50 mM.

of Wang et al., 1996 (12) that parallel surface and pore diffusion may be the dominant transport mechanism in adsorbents with high capacities.

Analysis of the various dimensionless groups enables one to choose an appropriate transport model for a given resin system. An illustration of this technique is provided here for the FF Sepharose material. As described above, parallel pore and surface diffusion are the dominant transport mechanisms in this resin. The kinetics of desorption, film mass transfer, and the axial dispersion

are clearly less important. Accordingly, for this resin system, the transport-dispersive model (Eqs. 5 and 6) was employed. The mass transfer coefficient employed in these equations is a lumped coefficient reflecting contributions from both pore and surface diffusion.

Displacement experiments were carried out at two different loadings to enable a comparison with model predictions. The results are shown in Figs. 5(a–b). As can be seen in the figures, there is excellent agreement between

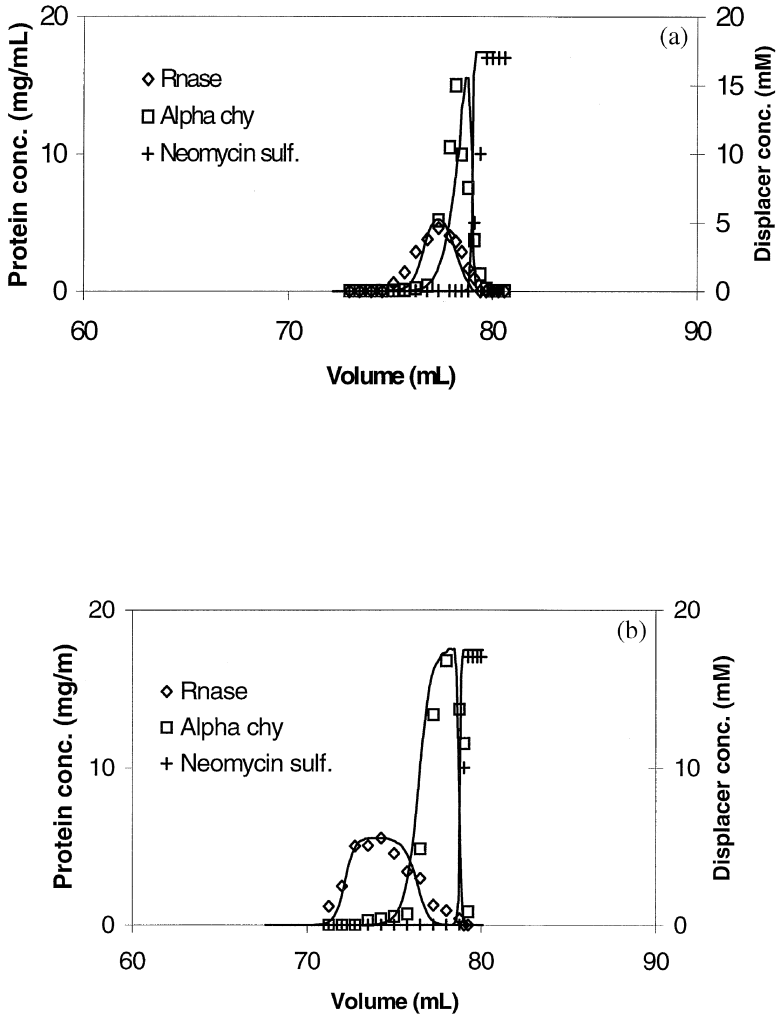


FIG. 5 Comparison of experimental and simulation results for the displacement separation of α-chymotrypsinogen A and ribonuclease A on FF Sepharose. Solid lines are simulation results. (a) Feed load: 12 mL; feed: 0.18 mM ribonuclease A and 0.22 mM α-chymotrypsinogen A in 50 mM phosphate buffer (pH 6); flow rate: 0.5 mL/min; fraction size: 500 μL; displacer: 17 mM neomycin sulfate in 50 mM phosphate buffer (pH 6). (b) Feed load: 34 mL; feed: 0.19 mM ribonuclease A and 0.17 mM α-chymotrypsinogen A in 50 mM phosphate buffer (pH 6); flow rate: 0.5 mL/min; fraction size: 500 μL; displacer: 17 mM neomycin sulfate in 50 mM phosphate buffer (pH 6).





MARCEL DEKKER, INC.
270 Madison Avenue, New York, New York 10016

simulation and experimental results using no adjustable parameters. At low loadings, Fig. 5(a), the displaced protein zones are not sufficiently wide to produce pure material on this large particle diameter system. On the other hand, at higher loadings (Fig. 5b), a significant amount of pure material can be obtained. Again, the selected model can readily predict this behavior. These results validate the model employed to describe the chromatographic behavior of solutes in this resin system.

## CONCLUSIONS

A simple methodology was presented for the characterization of various ion-exchange materials. Pulse injections were made under retained and unretained conditions at various flow rates. This enabled the generation of a set of HETP plots as a function of both the linear velocity and the salt concentration. By fitting the plots using the developed equations, one could then estimate the relevant transport properties for a given protein on a specific resin system. By evaluating the variation of the slope of the HETP plots as a function of the salt concentration, one could also obtain the relative importance of surface diffusion effects on a specific resin. Indeed, the results indicate that in high capacity resins, such as HP and FF Sepharose materials, surface diffusion effects can be significant. The appropriate dimensionless groups were then determined to analyze the relative rates of the various transport mechanisms and to select an appropriate model. Comparisons between simulation and experimental results were provided to illustrate the use of this methodology. The present body of work provides a useful tool for determining both the parameters and the appropriate models for simulating preparative ion-exchange chromatography. Furthermore, this approach provides insight into the relative importance of different transport mechanisms in ion-exchange resins. Finally, this methodology now enables comparison of the performance of different preparative modes (e.g., displacement and gradient chromatography) on various ion-exchange resin systems. This will be the subject of a future report.

## NOMENCLATURE

| | |
|---|---|
| $b_0$ | parameter reflecting retention factor |
| $C$ | mobile phase concentration (mM) |
| $d_p$ | particle diameter (cm) |
| $D_a$ | axial dispersion coefficient ($cm^2/s$) |
| $D_m$ | molecular diffusivity ($cm^2/s$) |
| $D_p$ | pore diffusion coefficient ($cm^2/s$) |
| $D_s$ | surface diffusion coefficient ($cm^2/s$) |





MARCEL DEKKER, INC.
270 Madison Avenue, New York, New York 10016

| | |
|---|---|
| $F$ | flow rate (mL/min) |
| $H$ | height equivalent to a theoretical plate (cm) |
| $k'_{des}$ | desorption rate constant ($mM^{-v} \cdot s^{-1}$) |
| $k_f$ | film transport coefficient (cm/s) |
| $k_m$ | lumped mass transport coefficient ($s^{-1}$) |
| $K_{SMA}$ | equilibrium constant in SMA formalism |
| $L$ | length of column (cm) |
| Pe | Peclet number ($= Lu/D_a$) |
| $Q$ | stationary phase concentration (mM) |
| $r$ | ratio of surface diffusion and pore diffusion |
| $R$ | particle radius (cm) |
| Re | Reynolds number ($= ud_p/\eta$) |
| $S$ | slope of HETP vs $u$ plots |
| Sc | Schmidt number ($= \eta/D_m$) |
| Sh | Sherwood number ($= k_f d_p/D_m$) |
| St | Stanton number ($= k_m L/u$) |
| $t_{w,0.5}$ | width at half-height (min) |
| $t_r$ | retention time (min) |
| $u$ | superficial velocity (cm/s) |
| $V_0$ | column dead volume (mL) |
| $x$ | dimensionless axial distance |

### *Greek*

| | |
|---|---|
| $\beta$ | phase ratio [$= (1 - \varepsilon_i)/\varepsilon_i$] |
| $\varepsilon_i$ | interstitial porosity |
| $\varepsilon_p$ | particle porosity |
| $\varepsilon_t$ | total porosity |
| $\eta$ | kinematic viscosity ($cm^2/s$) |
| $\nu$ | characteristic charge |
| $\mu_1$ | first moment |
| $\sigma$ | steric factor |
| $\sigma_{ec}$ | square root of variance (min) |
| $\tau_{tor}$ | tortuosity factor |
| $\tau$ | dimensionless time |
| $\zeta$ | axial dispersion parameter (cm) |
| $\Lambda$ | ionic capacity (mM) |

## ACKNOWLEDGMENTS

The authors acknowledge the National Science Foundation (Grant CTS-9416921) and Amersham Pharmacia Biotech for their support of this research.

## REFERENCES


1. N. B. Afeyan, S. P. Fulton, and F. E. Regnier, *J. Chromatogr., 544*, 267–279 (1991).
2. P. Miroslav, S. Frantisek, and J. M. J. Frechet, *J. Chromatogr. A, 752*, 59–66 (1996).
3. E. Boschetti, *Ibid., 658*, 207–236 (1994).
4. J. Horvath, E. Boschetti, L. Guerrier, and N. Cooke, *Ibid., 679*, 11–22 (1994).
5. P. R. Levison, R. M. H. Jones, D. W. Toome, S. E. Badger, M. Streater, and N. D. Pathirana, *Ibid., 734*, 137–143 (1996).
6. P. R. Levison, C. Mumford, M. Streater, A. Brandt-Nielsen, N. D. Pathirana, and S. E. Badger, *Ibid., 760*, 151–158 (1997).
7. D. C. Nash and H. A. Chase, *Ibid., 807*, 185–207 (1998).
8. C. A. Brooks and S. M. Cramer, *AIChE J., 38*, 1969–1978 (1992).
9. S. R. Gallant, A. Kundu, and S. M. Cramer, *J. Chromatogr., A, 702*, 125–142 (1995).
10. S. R. Gallant, S. Vunnum, and S. M. Cramer, *Ibid., 725*, 295–314 (1996).
11. S. R. Gallant, A. Kundu, and S. M. Cramer, *Biotechnol. Bioeng., 47*, 355–372 (1995).
12. Z. Ma, R. D. Whitley, and N.-H. L. Wang, *AIChE J., 42*, 1244–1262 (1996).
13. C. K. Lee, Q. Yu, S. U. Kim, and N.-H. L. Wang, *J. Chromatogr., 484*, 29–59 (1989).
14. R. D. Whitley, K. E. Van Cott, and N.-H. L. Wang, *Ind. Eng. Chem. Res., 32*, 149–159 (1993).
15. J. A. Berninger, R. D. Whitley, X. Zhang, and N.-H. L. Wang, *Comput. Chem. Eng., 15*, 749–768 (1991).
16. F. H. Arnold, H. W. Blanch, and C. R. Wilke, *Chem. Eng. J., 30*, B25–B36 (1985).
17. P. Schneider and J. M. Smith, *AIChE J., 14*, 886–895 (1968).
18. J. J. van Deemter, F. J. Zuiderweg, and A. Klinkenberg, *Chem. Eng. Sci., 5*, 271–289 (1956).
19. J. C. Giddings, *Dynamics of Chromatography, Part I*, Dekker, New York, NY, 1965.
20. Cs. Horvath and H.-J. Lin, *J. Chromatogr., 149*, 43–70 (1978).
21. J. H. Knox and H. P. Scott, *Ibid., 282*, 297–313 (1983).
22. D. D. Frey, E. Schweinheim, and Cs. Horvath, *Biotechnol. Prog., 9*, 273–284 (1993).
23. A. E. Rodrigues, A. M. D. Ramos, J. M. Loureiro, M. Diaz, and Z. P. Lu, *Chem. Eng. Sci., 47*, 4405–4413 (1992).
24. A. E. Rodrigues, Z. P. Lu, J. M. Loureiro, and G. Carta, *J. Chromatogr. A, 653*, 189–198 (1993).
25. A. Velayudhan, "Studies in Nonlinear Chromatography," Doctoral Dissertation, Yale University, New Haven, CT, 1990.
26. G. Guiochon, S. Golshan Shirazi, and A. M. Katti, *Fundamentals of Preparative and Nonlinear Chromatography*, Academic Press, New York, NY, 1994.
27. S. C. Foo and R. G. Rice, *AIChE J., 21*, 1149–1158 (1975).
28. S. D. Gadam, G. Jayaraman, and S. M. Cramer, *J. Chromatogr., 630*, 37–52 (1993).
29. A. Kundu, "Low Molecular Weight Displacers for Protein Purification in Ion Exchange Systems," Doctoral Dissertation, Rensselaer Polytechnic Institute, Troy, NY, 1996.
30. V. Natarajan and S. M. Cramer, *AIChE J., 45*, 27–37 (1999).
31. A. Kundu, A. A. Shukla, K. A. Barnthouse, J. Moore, and S. M. Cramer, *BioPharm, 10*, 64–70 (1997).
32. G. Carta, Prep '97 Workshop, 1997.
33. M. T. Tyn and T. W. Gusek, *Biotechnol. Bioeng., 35*, 327–338 (1990).


*Received by editor June 19, 1999*
*Revision received August 1999*





MARCEL DEKKER, INC.
270 Madison Avenue, New York, New York 10016

# Request Permission or Order Reprints Instantly!